Use of Isotropically Tumbling Bicelles to Measure Curvature Induced by Membrane Components

ARTICLE *in* LANGMUIR · SEPTEMBER 2014

Impact Factor: 4.46 · DOI: 10.1021/la5030668 · Source: PubMed

3 AUTHORS, INCLUDING:

Sean Thomas Smrt
University of Illinois at Chicago
4 PUBLICATIONS **4** CITATIONS

Langmuir

Article

pubs.acs.org/Langmuir

Use of Isotropically Tumbling Bicelles to Measure Curvature Induced by Membrane Components

Adrian W. Draney, Sean T. Smrt, and Justin L. Lorieau*

Department of Chemistry, University of Illinois at Chicago, Chicago Illinois 60607, United States

Supporting Information

ABSTRACT: Isotropically tumbling discoidal bicelles are a useful biophysical tool for the study of lipids and proteins by NMR, dynamic light scattering, and small-angle X-ray scattering. Isotropically tumbling bicelles present a low-curvature central region, typically enriched with DMPC in the lamellar state, and a highly curved detergent rim, typically composed of DHPC. In this report, we study the impact of the partitioning and induced curvature of a few molecules of a foreign lipid on the bicelle size, structure, and curvature. Previous approaches for studying curvature have focused on macroscopic and bulk properties of membrane curvature. In the approach presented here, we show that the conical shape of the DOPE lipid and the inverted-conical shape of the DPC lipid induce measurable curvature changes in the bicelle size. Bicelles with an average of 1.8 molecules of DOPE have marked increases in the size of bicelles, consistent with negative membrane curvature in the central region of the bicelle. With bicelle curvature models, radii of curvature on the order of −100 Å and below are measured, with a greater degree of curvature observed in the more pliable L_α state above the phase-transition temperature of DMPC. Bicelles with an average of 1.8 molecules of DPC are reduced in size, consistent with positive membrane curvature in the rim, and at higher temperatures, DPC is distributed in the central region to form mixed-micelle structures. We use translational and rotational diffusion measurements by NMR, size-exclusion chromatography, and structural models to quantitate changes in bicelle size, curvature, and lipid dynamics.

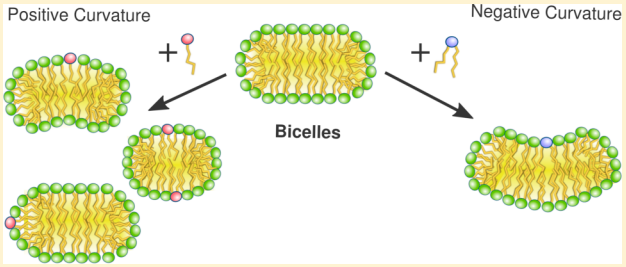

INTRODUCTION

Phospholipids are fundamental biomolecules in the compartmentalization and transfer of molecules in cells. In an aqueous environment, phospholipids self-assemble into membranes and closed structures, isolating their hydrophobic tails and exposing their hydrophilic headgroups to water. When bilayer-forming phospholipids are solubilized by detergents, bilayered mixed micelles known as bicelles form in a variety of morphologies.[1,2] Bicelles are commonly composed of dimyristoylphosphocholine (DMPC) as the bilayer-forming lipid and dihexanoylphosphocholine (DHPC) or the ether-linked variant as the detergent lipid, yet a number of detergent and lipid compositions have been reported.[3−7] Bicelle morphology is dictated by the hydration, temperature, and ionic strength but most importantly the molar concentration ratio of the bilayer-forming or long-chain lipid to the detergent lipid, denoted as the q ratio.[8] At high q ratios, lamellar structures dominate, forming perforated lamellar sheets of DMPC with toroidal pores lined by DHPC. These sheets align in a magnetic field and have been used extensively for the measurement of residual dipolar couplings (RDC) of proteins in liquid-state NMR as well as in structural analyses of membrane proteins by solid-state NMR (SSNMR).[9−11] At lower q ratios, typically below 2.5, bicelles form small phase-separated aggregates with a disk shape composed of a planar central region enriched in the long-chain lipid and a highly curved toroidal rim enriched in the detergent lipid.[5,6]

Small bicelles have been widely adopted in the biophysical characterization of membrane proteins as they present a nativelike bilayer environment to proteins yet tumble rapidly and isotropically, making them suitable for liquid-state NMR, dynamic light scattering (DLS), and small-angle X-ray and neutron scattering (SAXS and SANS) experiments.[12,13] The composition and size of isotropically tumbling DMPC/DHPC bicelles depend on the temperature, lipid concentration, and q ratio, with bicelles at high lipid concentrations and q ratios of 0.5 producing monodisperse samples and larger bicelles (q > 1.0) at lower lipid concentrations producing polydisperse samples.[14] A fraction of the detergent lipid typically remains unbound from the bicelles and free in solution, and dilution increases the effective q ratio (q_e) to produce larger discoidal particles.[15] The free concentration of DHPC, $[DHPC]_{free}$, varies with the q ratio, and ^{31}P chemical shift and diffusion-ordered spectroscopy (DOSY) NMR experiments have measured these in the range of 6−12 mM. A $q_e$ratio is commonly used to measure the effective bicelle size from the reduced concentration of DHPC bound to the bicelle.

Received: May 22, 2014
Published: September 9, 2014

The structure and colloidal properties of bicelles is an active field of investigation. The partitioning of foreign lipids and proteins and the coupling among the molecular shape, membrane curvature, and bicelle size remain poorly understood. In membranes, curvature is an important factor in driving the interactions between membranes and in defining the structure of organelles.[16] The spontaneous curvature of a membrane is dictated by the shape and aggregation of the constituent lipids. Lipids and proteins have either an inverted conical, conical, or cylindrical shape.[17,18] The shape of phospholipids is largely determined by the volume and cross-sectional area of the hydrophilic headgroup in relation to the hydrophobic tail of the molecule.[18] Longer lipid chains composed of 14 or more carbons and cis-unsaturated double bonds increase the volume of the lipid tail region. The headgroup volume is increased by the number of methyl groups or other bulky substituents in this region. The inverted conical lipid DHPC has shorter six-carbon aliphatic chains, and dodecylphosphocholine (DPC) has a singly branched aliphatic chain, and the volume of the hydrophobic tail region is smaller for these molecules in proportion to their hydrophilic phosphocholine headgroup. Inverted conical lipids spontaneously form micelle structures in an aqueous environment and aggregate on the rim of bicelle aggregates. Cylindrical lipids, such as DMPC, dipalmitoylphosphocholine (DPPC), and palmitoyloleoylphosphocholine (POPC), have a uniform volume from the headgroup to the tail, producing a cylindrical shape. Cylindrical lipids have a high propensity to form lamellar structures, and these aggregate in the central region of bicelle structures. Cone-shaped lipids, such as the dioleoylphosphoethanolamine (DOPE) lipid with cis-unsaturated 18-carbon aliphatic chains, have a larger volume in the aliphatic region than the hydrophilic headgroup, and these spontaneously form hexagonal and cubic inverted structures in an aqueous environment.[18] The morphology of membrane aggregates formed by these lipids is characterized by either positive, negative, or neutral (zero) curvature and a radius of curvature (R_c) along each of the two axes in the plane of the membrane. Positive curvature is defined by convex monolayers, which are spontaneously formed by inverted-cone shaped amphiphiles and lytic proteins such as MSI-78.[19] Negative curvature is defined by concave monolayers, which are spontaneously formed by cone-shaped amphiphiles and peptides such as the islet amyloid polypeptide and pardaxin.[20,21] As exemplified by the phase separation of DMPC and DHPC in isotropically tumbling bicelles, lipids become segregated in membranes based partially on the molecular shape.[22−24]

A variety of biophysical tools have studied the bulk structure and curvature of membranes. Crystallography experiments have measured the radii of curvature of lipids by tracking changes in the radial dimension of the hexagonally inverted state of DOPE by the introduction of added foreign lipids.[25−27] Crystallography has produced accurate radii of curvature for various lipids, but the method suffers from the utilization of the nonphysiological H_{II} state of DOPE. Fluorescence microscopy and atomic force microscopy (AFM) have established the importance of lipid sorting, protein crowding, and the energy needed to introduce curvature protrusion in vesicles.[28−31] Differential scanning calorimetry (DSC), Fourier transform infrared spectroscopy (FTIR), and SSNMR have measured how lipids of different shape change the bulk phase properties of membranes.[32,33] Moreover, SSNMR has been used qualitatively to measure changes in vesicle radii in the presence of amphipathic peptides[34,35]

In this report, we investigate the induction of membrane curvature and lipid sorting in isotropically tumbling bicelles. We study bicelle-induced curvature and sorting (BICS) to understand changes in the morphology and average size of bicelles in the presence of foreign, curvature-inducing lipids. By studying bicelles with an average of only a few molecules of the inverted-cone-shaped DOPE or the cone-shaped DPC molecule, we have found significant changes in the bicelle sizes and have related these changes to structural parameters with curvature models.

EXPERIMENTAL SECTION

Sample Preparation. DHPC, DOPE, DMPC, and DPC were purchased from Avanti Lipids and Anatrace and used without further purification. Oleic acid, deuterium oxide, and citrate were purchased from Sigma-Aldrich, and Tris base was purchased from Fisher Scientific.

For the NMR experiments, all bicelle samples were prepared in 25 mM Tris buffer pH 7.4, 90% H_2O, 10% D_2O. A stock bicelle solution with 55 ± 1 mM DMPC and 186 ± 3 mM DHPC (q = 0.30) was prepared. The stock solution was distributed in aliquots to make bicelle formulations match the concentration of the perturbing lipid and the total volume fraction of lipid. The following lipids were added to each aliquot: 10 ± 1 mM DMPC (DMPC-bicelle), 10 ± 1 mM DOPE (DOPE-bicelle), 11 ± 1 mM DHPC (DHPC-bicelle), and 11 ± 1 mM DPC (DPC-bicelle). Separately, bicelles with 54 ± 1 mM DMPC, 181 ± 3 mM DHPC (q = 0.30), and 8 ± 1 mM oleic acid (OA-bicelle) were prepared at pH 7.5 and pH 4.5 by titrating with 1 M citric acid. The absence of lipid degradation or hydrolysis was confirmed from ^{1}H and ^{31}P 1D NMR spectra. Concentrations of lipids were measured from the integrals of ^{31}P and ^{1}H 1D NMR spectra (Figure S2), with the exception of oleic acid, which was quantitated gravimetrically.

Bicelle titration studies were conducted by preparing a stock bicelle solution in 25 mM Tris buffer at pH 7.4 with 83 ± 2 mM DMPC and 163 ± 3 mM DHPC (q = 0.51) and distributing aliquots to make formulations of increasing DOPE concentration as well as a reference DMPC-bicelle sample. Measurements are reported at 30 °C. The following concentrations were added to each aliquot: 4 ± 1 mM DOPE, 9 ± 1 mM DOPE, and 21 ± 1 mM DOPE.

For the SEC experiments, a separate set of bicelle samples were prepared in 25 mM Tris buffer at pH 7.4. The stock bicelle solution included 28 ± 1 mM DMPC and 85 ± 1 mM DPC (q = 0.33) and was prepared with a 400 μM perylene probe for UV−vis detection. Excess perylene that was not dissolved in the bicelles was removed by centrifugation. The stock solution was distributed into aliquots to make matched bicelle formulations with increasing concentration of curvature-inducing lipid: 0, 1.5 ± 0.5, and 3.6 ± 0.5 mM DOPE. An additional set of bicelle samples was prepared in 25 mM Tris buffer at pH 7.4 with 39 ± 1 mM DMPC and 77 ± 1 mM DPC (q = 0.51) with 400 μM of perylene. This stock was distributed in aliquots to make matched bicelle formulations with 0 and 1.3 ± 0.5 mM DOPE. After the addition of DOPE, all samples were mixed with five freeze−thaw cycles and vortex mixing.

The chromatography mobile phase run buffer was prepared with 25 mM Tris pH 7.4 and 2 mM DPC to account for the free concentration of DPC present in the solution.[36]

In isotropically tumbling bicelles, a small fraction of the DHPC is partially miscible and in rapid exchange as a monomer in solution. This free concentration was calculated from the translational diffusion rates with equation (S1), and the values are listed in Table S2. An effective ratio, q_e, was used to account for the effective concentration of the detergent bound to bicelles.[3]

$$q_e = \frac{[\mathrm{DMPC}]}{[\mathrm{DHPC}] - [\mathrm{DHPC}]_{\mathrm{free}}} \quad (1)$$

dx.doi.org/10.1021/la5030668 | Langmuir 2014, 30, 11723−11733

NMR Experiments. Spectra were recorded on a Bruker Avance III HD 500 MHz NMR spectrometer using a QXI 500S1 quadruple resonance (^{1}H, ^{31}P, ^{13}C, ^{15}N) probe with triple-axis pulsed field gradients.

Diffusion measurements were conducted with a ^{1}H longitudinal eddy-current delay with a bipolar pulse-pair gradient (LED-BPP) diffusion experiment using a WATERGATE readout.[16] The LED and BPP together are used to minimize gradient eddy-current recovery times and produce more accurate diffusional rates.[16,37] Translational diffusion constants, D_t, were measured from a Gaussian fit of the intensity decay profiles, $I(f)$, as a function of the fractional gradient strength, f, using NMRPipe.[38]

$$\frac{I(f)}{I(f_0)} = \exp\left(-(\gamma\delta G_{max})^2(f^2 - f_0^2)\left(\Delta - \frac{\delta}{3} - \frac{\tau}{2}\right)D_t\right) \quad (2)$$

The gyromagnetic ratio, γ, of 2.675×10^8 s^{-1} T^{-1} for ^{1}H was used. Diffusion gradients were varied from 2 to 60% using a smoothed-square Chirp pulse amplitude on both the x and z gradients. A total of 16 gradient points were measured. A gradient pulse length, δ, of 2 ms, a diffusion period, Δ, and bipolar gradient correction delays, τ, of 800 ms and 200 μs, respectively, were used for the bicelle samples. The diffusion of DHPC and DMPC was followed by their resolved terminal $^{1}H_3C$ resonances, and the rate of diffusion for the bicelles was assumed to match that of DMPC.[15] DOPE contributes to the terminal $^{1}H_3C$ resonance of DMPC, but its contribution was less than 14.9% of the signal intensity and was therefore neglected. Samples were loaded into a Shigemi tube with a 14.0 ± 0.2 mm sample height.

Diffusion rates were measured from 15 to 40 °C in 5 °C increments with a 35 min pre-equilibrium time between experiments, and each experiment was repeated three to four times. It was found that at least one temperature cycle was needed to achieve consistent diffusional rates for the bicelles, and the first set was discarded. Average and standard deviations in the diffusion rates are reported, and a sample decay for the DOPE-bicelles is presented in Supporting Information Figure S3.

The DMPC ^{31}P R_2 and R_1 rates were measured from ^{31}P $T_{1\rho}$ and T_1 experiments, respectively.[39] A spin-lock field ν_1 of 1.00 kHz was used with spin-lock times of 6–200 ms. A ^{1}H decoupling field was achieved with a ν_1 of 625 Hz and a WALTZ-16 decoupling sequence. Further calibrations of the NMR experiments are included in the Supporting Information.

Size Exclusion Chromatography. Chromatograms were recorded on a GE ÄKTApurifier with a Superdex 200 GL 10/300 size exclusion chromatography column. Samples were injected in triplicate at a flow rate of 1.0 mL/min and eluted at an average temperature of 28.4 ± 0.5 °C. Calibration of the column used a series of protein standards of known molecular weight.[36]

RESULTS

The curvature of bicelles is measured by adding a small molar ratio of a curvature-perturbing lipid to the bicelles and comparing the change in the average size of the bicelles relative to a reference, unperturbed bicelle. The ratio between these two molecular weights is defined as the B ratio.

$$B = \frac{M_{w,curved}}{M_{w,reference}} \quad (3)$$

The curved and reference bicelle samples are made from the same stock solution with matching q_e ratios, and the reference bicelle is prepared by adding an equivalent amount of either DMPC or DHPC to match the lipid volume ratio of the curved bicelle.

Translational Diffusion. Translational diffusion is an accurate and unambiguous measure of the radius of hydration and size of phospholipid complexes. The translational self-diffusion of the bicelles was measured from the terminal methyl ^{1}H resonance of the DMPC lipid.[15] The translational diffusion rates are presented for the DMPC-, DHPC-, DPC-, and DOPE-bicelles over the range of 15–40 °C (Figure 1).

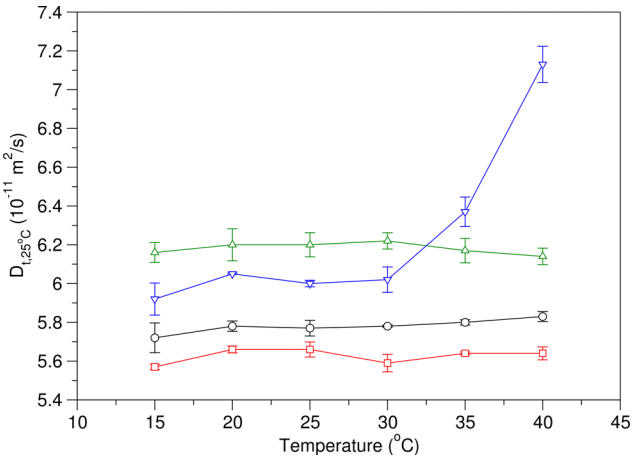

Figure 1. Bicelle translational diffusion measurements for the DMPC- (black, circle), DOPE- (red, square), DHPC- (green, triangle up), and DPC-bicelles (blue, triangle down). Translational diffusion rates were measured between 15 and 40 °C, and the self-diffusion rates have been corrected to the solvent viscosity and temperature at 25 °C. Translational diffusion rates of bicelles were measured from the terminal $^{1}H_3C$ resonance of DMPC using a ^{1}H DOSY NMR experiment. The lipid volume fractions of all bicelles have been matched to 12.0% (v/v). Sample composition details are described in the Experimental Section.

This temperature range crosses the gel (L_β) to liquid-crystalline (L_α) phase transition of DMPC at 23.6 °C.[40] The rates have been corrected and normalized for viscosity and temperature to a reference temperature of 25.0 °C ($D_{t,25\ °C}$). Consequently, these corrected translational diffusion rates remain constant when the bicelle size remains unchanged as a function of temperature, as observed with the DMPC-bicelles. The measured diffusion constant can be related to the self-diffusion constant at infinite dilution, D_0, for low volume fractions, $\Phi < 0.15$.

$$D_t = D_0(1 - 3.2\lambda\Phi) \quad (4)$$

The interaction volume shape factor, λ, is 0.95 ± 0.05 for DHPC/DMPC and DHPC/POPC bicelles with q = 0.15–0.53.[15] The densities of lipids are 1.11, 1.02, 1.13, 1.08, and 0.89 g/cm^3 for DHPC, DMPC, DOPE, DPC, and oleic acid, respectively.[41,42] The self-diffusion constant at infinite dilution can be related to the radius of hydration of a spherical particle, R_h, the viscosity, η, and the temperature of the solution with the Stokes–Einstein equation.

$$D_0 = \frac{kT}{6\pi\eta R_h} \quad (5)$$

For oblate spheroids, the rate of translational diffusion is further reduced by the Perrin shape factor, F, which is 1.0 for a hard sphere and at most 1.042 for a bicelle with q = 0.5.[15]

The average mass of the bicelle particles (in kDa) has a cubic relationship with the translational diffusion constant (in m^2/s)[15] over the bicelle size range of 21.7 to 67.2 kDa (q = 0.15–0.53). The B ratio is calculated from the translational diffusion rates of the curved and reference bicelles.

dx.doi.org/10.1021/la5030668 | Langmuir 2014, 30, 11723–11733

$$B_t = \left(\frac{D_{t,curved}}{D_{t,reference}}\right)^{-3} \quad (6)$$

The subscript t indicates the measurement of the B ratio from translational diffusion. We matched the volume fraction of lipids between bicelle samples, and the measured translational diffusion rate (D_t) at each temperature was used directly rather than the rate of diffusion at infinite dilution. The B ratio approximately cancels modest changes to the Perrin shape factor, the volume shape factor, the sample temperature, and the viscosities between reference and curved bicelle samples.

The DMPC-bicelles have translational diffusion rates of $D_{t,25\ °C} = (5.72 \pm 0.08) \times 10^{-11}$ m^2/s at 15 °C and $(5.83 \pm 0.03) \times 10^{-11}$ m^2/s at 40 °C, which indicates that the bicelles remain the same size within error over this temperature range. These diffusion rates correspond to an effective molecular weight of 20.3 kDa and a free concentration of DHPC of 10 ± 2 mM (details in the Supporting Information).

The DOPE-bicelles have an average of 1.8 molecules per bicelle ($\chi_{DOPE\text{-}bicelle} = 1.8$). The DMPC and DHPC chemical shifts and the diffusion curves are uniform, indicating a homogeneous, ensemble-averaged bicelle size in rapid exchange on the NMR time scale (Figures S2 and S3). The translational diffusion $D_{t,25\ °C}$ rates for the DOPE-bicelles are $(5.57 \pm 0.01) \times 10^{-11}$ m^2/s at 15 °C and $(5.64 \pm 0.03) \times 10^{-11}$ m^2/s at 40 °C, and $[DHPC]_{free}$ is 10 ± 2 mM over these temperatures. The translational diffusion rates of the DOPE-bicelles are consistently smaller than those of the DMPC-bicelles, indicating that DOPE induced an average increase in bicelle size by 8 ± 4% ($B_t = 1.08 \pm 0.04$) at 15 °C and 11 ± 3% ($B_t = 1.11 \pm 0.03$) at 40 °C. The molecular weight difference between DOPE and DMPC molecules would account for a change in size by only ca. 210 Da, or an increase of 0.8% in bicelle size.

A titration of the average number of DOPE molecules per bicelle was conducted for larger bicelles with a q_e of 0.54 (Figure 3b). Bicelles were titrated to contain an average of 0.8, 1.9, or 6.0 molecules of DOPE. At 30 °C, these bicelles have $D_{t,25\ °C}$ rates of $(5.24 \pm 0.03) \times 10^{-11}$ m^2/s, $(5.09 \pm 0.06) \times 10^{-11}$ m^2/s, and $(4.49 \pm 0.02) \times 10^{-11}$ m^2/s, and $[DHPC]_{free}$ remains constant at 8 ± 2 mM. These bicelles are consistently larger than the reference bicelles by 19 ± 5% ($B_t = 1.19 \pm 0.05$), 38 ± 6% ($B_t = 1.38 \pm 0.06$), and 121 ± 4% ($B_t = 2.21 \pm 0.04$) for bicelles with averages of 0.8, 1.9, and 6.0 molecules of DOPE, respectively. The increase in bicelle size and B_t ratios follow a linear relationship with the average number of DOPE molecules per bicelle.

The DHPC-bicelles have $D_{t,25\ °C}$ rates that range from $(6.16 \pm 0.05) \times 10^{-11}$ m^2/s at 15 °C to $(6.14 \pm 0.04) \times 10^{-11}$ m^2/s at 40 °C, and $[DHPC]_{free}$ increases slightly from 9 ± 2 to 11 ± 2 mM over this temperature range. The DHPC-bicelles remain the same size from 15 to 40 °C, and these are smaller than the DMPC-bicelles by 10−14% ($B_t = (0.86\text{−}0.90) \pm 0.02$).

By contrast, the DPC-bicelles have an average of 1.8 molecules per bicelle ($\chi_{DPC\text{-}bicelle} = 1.8$), and these bicelles have $D_{t,25\ °C}$ rates that range from $(5.92 \pm 0.08) \times 10^{-11}$ m^2/s at 15 °C to $(7.13 \pm 0.09) \times 10^{-11}$ m^2/s at 40 °C. $[DHPC]_{free}$ remains constant at 9 ± 2 mM from 15 to 40 °C. The DPC-bicelles are consistently smaller than the DMPC-bicelles at all measured temperatures. The DPC-bicelles are smaller than the DMPC-bicelles by 10 ± 5% ($B_t = 0.90 \pm 0.05$) at 15 °C and smaller by 45 ± 2% ($B_t = 0.55 \pm 0.02$) at 40 °C.

In comparison to the DHPC-bicelles, the DPC-bicelles are larger by 12 ± 6% ($B_t = 1.12 \pm 0.06$) at 15 °C and smaller by 36 ± 3% ($B_t = 0.64 \pm 0.03$) at 40 °C. The molecular weight difference between DPC and DHPC would account for a decrease in bicelle size of only ca. 224 Da (1%).

The larger bicelle size for the DPC-bicelles in comparison to that for the DHPC-bicelles at the lower temperature agrees with the larger radius of curvature for the DPC molecule in comparison to that for DHPC.[42] As discussed below, the progressive decrease in bicelle size as the temperature is increased is consistent with a partial partitioning of the DPC molecules from the rim to the central region of the bicelle at the higher temperatures and demonstrates that DPC further reduces the size of bicelles. This is furthermore supported by a higher affinity for the DHPC to the bicelles and a lower $[DHPC]_{free}$ at temperatures above 30 °C for the DPC-bicelles (Figure S4).

The translational diffusion rates were measured as a function of pH for the OA-bicelles (oleic acid) at 30 °C for an average molar ratio, $\chi_{OA\text{-}bicelle}$, of 1.1 molecules per bicelle. Oleic acid induces negative curvature and membrane fusion in a pH-dependent manner.[43] Below pH 5.7−6.3, oleic acid is protonated and partitions more deeply in the phospholipid membrane. At pH 7.5, the OA-bicelle $D_{t,25\ °C}$ is $(6.38 \pm 0.12) \times 10^{-11}$ m^2/s, and at pH 4.5, the $D_{t,25\ °C}$ is $(6.16 \pm 0.15) \times 10^{-11}$ m^2/s. The bicelles at low pH are 11 ± 10% ($B_t = 1.11 \pm 0.10$) larger and indicate that the oleic acid induces an increase in bicelle size at the lower pH.

Rotational Diffusion. Rotational diffusion from ^{31}P relaxation measurements of DMPC are sensitive to the overall tumbling time (τ_m) and the size of the bicelle as well as changes in the internal dynamics of the DMPC lipid molecules. In comparison to the translational diffusion data, which are sensitive only to changes in bicelle size, the ^{31}P relaxation measurements can therefore be used as a measure of the changes in the dynamics of the DMPC lipid.

The DMPC ^{31}P R_1 and R_2 relaxation rates are calculated from the relaxation contributions of the chemical shift anisotropy (CSA) and ^{1}H−^{31}P dipolar interactions.[44]

$$R_1 = \sum_{dipoles} d_i^2(J(\omega_H - \omega_P) + 3J(\omega_P) + 6J(\omega_H + \omega_P)) + c^2 J(\omega_P) \quad (7)$$

$$R_2 = \sum_{dipoles} \frac{1}{2} d_i^2(4J(0) + J(\omega_H - \omega_P) + 3J(\omega_P) + 6J(\omega_H) + 6J(\omega_H + \omega_P)) + \frac{1}{6} c^2(3J(\omega_P) + 4J(0)) \quad (8)$$

The dipolar constant, d_i^2, is $0.1\gamma_H^2\gamma_P^2\hbar^2\langle 1/r_{HP}^3\rangle$ in which γ is the gyromagnetic ratio, $\hbar$ is Planck's constant, and r_{HP} is the internuclear distance between ^{1}H and ^{31}P nuclei. The strength of the dipolar coupling is independent of the applied field strength, B_0, and multiple weak dipolar couplings from the ^{31}P nucleus to the choline H^α/H^β and glycerol $H^{G1}/H^{G2}/H^{G3}$ protons contribute. The CSA constant, c^2, is $(2/15)\text{-}\gamma_P^2 B_0^2(\Delta\sigma_P)^2$ in which $\Delta\sigma_P$ is the anisotropy of the ^{31}P CSA tensor, and the CSA contribution to the relaxation has a quadratic dependence on the applied magnetic field strength. The $\Delta\sigma_P$ is motionally averaged and has a value of ca. 47 ppm in the L_α phase of DMPC.[45] Fast time scale motions that contribute to the narrowing of the CSA and dipolar interactions

dx.doi.org/10.1021/la5030668 | Langmuir 2014, 30, 11723−11733

include lipid wobbling and undulation motions of the membrane.[46,47]

The relaxation rates depend on the spectral densities of motion, $J(\omega)$, at multiples of the Larmor frequencies for the ^{1}H and ^{31}P nuclei. The relaxation rates can be further simplified to better isolate the contribution of the $J(0)$ spectral density[48] and the motion of overall tumbling for the bicelles.

$$2R_2 - R_1 = \sum_{\text{dipoles}} d_i^2(4J(0) + 6J(\omega_H)) + \frac{4}{3}c^2J(0) \quad (9)$$

The measurement of the B_0 field dependence indicates that the CSA term accounts for ca. 90% of the ^{31}P $2R_2 - R_1$ rate for a ^{1}H field strength of 500 MHz.[49] The $J(0)$ spectral density dominates this relaxation and can be determined approximately using the Lipari–Szabo formalism.[50]

$$J(0) = \frac{2}{5}S^2\tau_m \quad (10)$$

This spectral density assumes that the overall tumbling time, τ_m, is much slower than the internal wobbling motion of the lipid, which for DMPC in isotropically tumbling bicelles is a reasonable approximation.[49] The order parameter, S^2, is the motional and ensemble average of the second Legendre polynomial for the reorientation of either the CSA or dipolar tensor. Its value ranges from 1.0 in the absence of reorienting motions to 0.0 for isotropic averaging.

Bicelles are oblate spheroids that tumble approximately isotropically, and the overall tumbling time is directly proportional to the average mass of the bicelle.[15] The DMPC ^{31}P relaxation rates can therefore be used to track changes in bicelle size and the B ratio as well as changes in the local dynamics of the DMPC lipids.

The ^{31}P $2R_2 - R_1$ rates for DMPC in the DMPC-, DOPE-, DPC-, and DHPC-bicelles are presented in Figure 2. The DMPC-bicelles do not change in size over this temperature range, according to translational diffusion measurements, yet

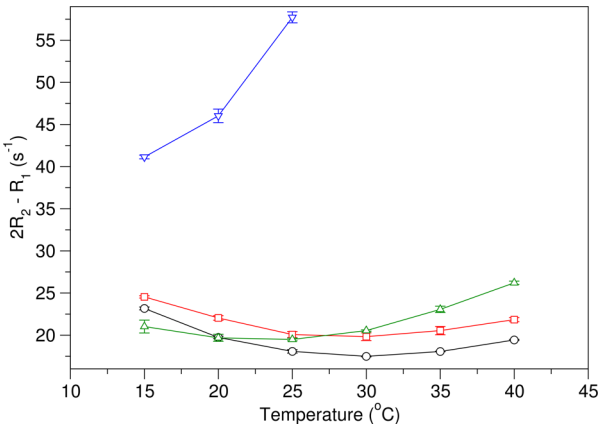

Figure 2. Bicelle DMPC ^{31}P relaxation rate measurements for the DMPC- (black, circle), DOPE- (red, square), DHPC- (green, triangle up), and DPC-bicelles (blue, triangle down). The ^{31}P relaxation rates report on motions that reorient the DMPC lipid molecule and the rotational diffusion of the bicelle. Relaxation rates were measured as a function of temperature. The lipid volume fractions of all bicelles have been matched to 12.0% (v/v). The DMPC and DHPC ^{31}P resonances for the DPC-bicelles coalesce above 25 °C, and the ^{31}P relaxation rates for DMPC could not be determined above this temperature. Sample composition details are described in the Experimental Section.

the ^{31}P $2R_2 - R_1$ rates for these bicelles vary by 23%. These rates are sensitive to changes in temperature and viscosity as well as changes in the amplitude of DMPC reorientations in the bicelle. However, the dependence of viscosity and temperature, which have a linear and inversely linear dependence on rotational diffusion,[51] and modest changes in the Perrin shape factor between reference and curved bicelles are canceled by taking the B_r ratio between bicelles.

$$B_r = \frac{2R_{2,\text{curved}} - R_{1,\text{curved}}}{2R_{2,\text{reference}} - R_{1,\text{reference}}} \approx \frac{S_{\text{curved}}{}^2\tau_{m,\text{curved}}}{S_{\text{reference}}{}^2\tau_{m,\text{reference}}} \quad (11)$$

The B ratios for the DOPE-bicelles are presented in Figure 3. The B_r ratio is 1.06 ± 0.04 at 15 °C and 1.12 ± 0.01 at 40 °C. These are within the error of the values measured from translational diffusion, confirming an increase in size for the DOPE-bicelles. However, the B ratios from rotational diffusion appear to increase at a lower temperature, possibly indicating a small change in DMPC lipid ordering ($S_{\text{curved}}{}^2/S_{\text{reference}}{}^2$) for the DOPE-bicelles near the phase-transition temperature of DMPC.

The $2R_2 - R_1$ rates for the DPC-bicelles are significantly larger than those from the DHPC-bicelles. These rates could not be measured above 25 °C because the DMPC and DHPC ^{31}P resonances coalesce above this temperature and are indistinguishable. The B_r ratios of DPC- to DHPC-bicelles at 15 and 20 °C are 1.92 ± 0.07 and 2.28 ± 0.06, respectively, which are significantly larger than those predicted by size alone in the translational diffusion measurements. The elevated ^{31}P R_2 rates of DMPC (Table S1) are also consistent with the mixing of DPC in the DMPC central region of the bicelle. Either chemical exchange contributions to the DMPC ^{31}P R_2 rate[40] or ordering of the DMPC molecules ($S_{\text{curved}}{}^2$) on a fast time scale is occurring in the presence DPC. The absence of relaxation dispersion for ^{31}P spin-lock fields between 1 and 2 kHz indicates that a chemical exchange mechanism would be much faster than the millisecond time scale. As a result, the elevated ^{31}P R_2 rates of DMPC suggest a mixing and ordering of the DMPC in the presence of DPC.

Size-Exclusion Chromatography. The size of bicelles was measured by size-exclusion chromatography (SEC). This technique has been previously used to characterize the sizes of lecithin–bile salt mixed micelles[37] and to monitor the dispersity of bicelle samples.

To maintain the size of the phospholipid aggregates, the run buffer included the free concentration of the short-chain lipid. In our experiments, we therefore used DMPC/DPC bicelles instead of the DMPC/DHPC bicelles of the above experiments because $[\text{DPC}]_{\text{free}}$ is much lower (<2 mM) than $[\text{DHPC}]_{\text{free}}$ (~10 mM).[15,42] We further integrated a small amount of the highly hydrophobic perylene molecule into the bicelles to be used as a tracer molecule and monitor bicelle elution.

The SEC elution profiles for the DMPC/DPC bicelles with DOPE are presented in the Supporting Information (Figure S6), and the bicelle sizes are presented in Table 1. The SEC chromatograms were repeated in triplicate for each sample, and they show a high degree of reproducibility. The DMPC/DPC bicelles are larger by a factor of ca. 2 compared to the DMPC/DHPC bicelles of the translational and rotational diffusion experiments, which is in agreement with previous observations[7] and the larger radius of curvature for the DPC molecules in comparison to the DHPC molecules.[42] These chromatograms

dx.doi.org/10.1021/la5030668 | Langmuir 2014, 30, 11723–11733

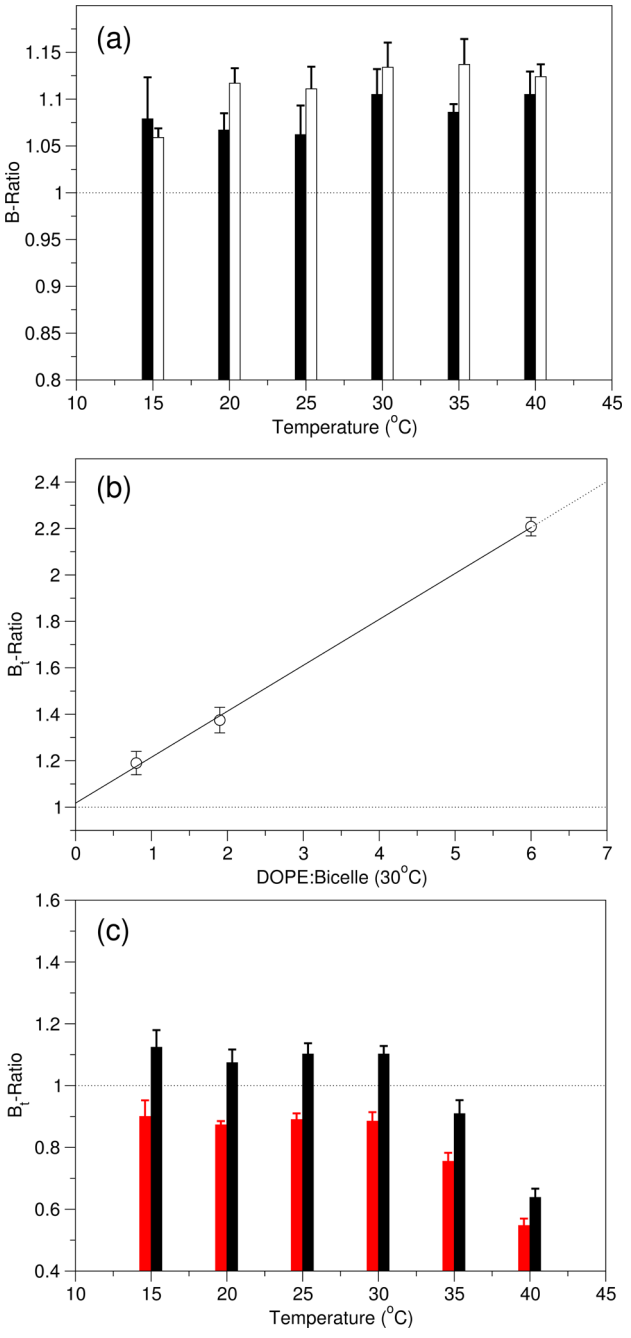

Figure 3. B ratios from translational diffusion (B_t, solid bars) and rotational diffusion (B_r, open bar) measurements. (a) The B ratios for the DOPE-bicelles in relation to the DMPC-bicelle reference are shown. (b) The B ratios for the DOPE titration in relation to the DMPC-bicelle reference at 30 °C. The linear regression fit in the B_t ratios is $B_t = 0.198x_{DOPE} + 1.017$. (c) The B_t ratios of the DPC-bicelles in relation to the DMPC-bicelle reference (red bars) and DHPC-bicelle reference (black bars) are shown. The B_t ratios from the translational diffusion were calculated with eq 6, and the B_r ratios from the rotational diffusion were calculated with eq 12. All bicelles have been matched in the volume fraction of lipid.

further demonstrate that the bicelles are monodisperse and homogeneous.

As the average number of DOPE molecules per bicelle increases, the size of the DMPC/DPC bicelles consistently increases. We measured increases in bicelle size for DMPC/DPC bicelles in the presence of DOPE for q = 0.33 and 0.51 bicelles. For the q = 0.33 bicelles, the DOPE to bicelle molecular ratios ($\chi_{DOPE\text{-}bicelle}$) are on average 2.6 and 6.0 molecules per bicelle, and these bicelles increase in size by 4.1 ± 1.0 and 8.1 ± 1.3 kDa, respectively, relative to the DPC/DMPC bicelles without DOPE. In contrast to the NMR experiments in which an equivalent number of molecules of DMPC or DHPC was been added to the reference bicelles when compared to the DOPE- and DPC-bicelles, the size increase from the added DOPE must be accounted for in the calculation of the chromatographic B_c ratios. We subtracted this contribution, and the corresponding q_e = 0.34 DMPC/DPC bicelles with an average of 2.6 and 6.0 molecules of DOPE per bicelle are 3 ± 1% (B_c = 1.03 ± 0.01) and 5 ± 2% (B_c = 1.05 ± 0.02) larger, respectively.

Table 1. Size of DPC/DMPC Bicelles Measured from Size-Exclusion Chromatography

bicelle	$\chi_{DOPE\text{-}bicelle}$	$V_{elution}$ (mL)	MW (kDa)	B_C[a]
q = 0.33	0.0	14.117 ± 0.015	76.5 ± 0.5	
	2.6	14.003 ± 0.025	80.6 ± 0.9	1.027 ± 0.013
	6.0	13.900 ± 0.030	84.6 ± 1.2	1.045 ± 0.017
q = 0.50	0.0	13.790 ± 0.026	89.0 ± 1.1	
	2.2	13.703 ± 0.032	92.6 ± 1.4	1.021 ± 0.017

[a] B_C is the ratio of the molecular weight for the bicelles with DOPE to the reference bicelle without DOPE. The additional molecular weight contribution from the DOPE molecules has been subtracted in the calculation of these ratios.

These results are consistent with our translational and rotational diffusion results, which show an increase in bicelle size in the presence of an average of a few molecules of DOPE per bicelle. However, the size increase per molecule of DOPE is smaller in the DPC/DMPC bicelles than in the DHPC/DMPC bicelles.

DISCUSSION

Partitioning and Dispersity. The molecular ratio of perturbing lipid to bicelle is expected to follow a Poisson distribution which predicts that an average molar ratio of 1.8 produces a distribution of bicelles with either no molecules (16.5%) or with one (29.8%), two (26.8%), three (16.1%), or more molecules of DOPE or DPC per bicelle. Accordingly, an instantaneous picture of this mixture would give a distribution of bicelle sizes and diffusion rates, depending on the number of DOPE or DPC lipids in any given bicelle.

The analysis of bicelle sizes is greatly simplified in our experiments because we measure average and effective bicelle sizes. On the milliseconds to minutes time scale of the experiments conducted in this study, homogeneous and monodisperse bicelles are observed, which is consistent with an effective bicelle size in rapid exchange. The translational diffusion experiments are accurately fit by a single translational diffusion rate in eq 2 (Figure S3), and the mixing time of 800 ms in these experiments is sufficient for the rapid exchange between bicelles, leading to a homogeneous ensemble-averaged bicelle size with an average of 1.8 molecules of DOPE or DPC per bicelle. If exchange were slower than this time scale, then the PFG gradient curves would require a distribution of diffusion rates to fit the data. Likewise, a single ^{31}P resonance and relaxation rate is observed for the DMPC and DHPC lipids in all bicelle samples (Figure S2). If the distribution of bicelles were in slow exchange, then a multiexponential fit would have been needed to fit the relaxation data. Finally, a single average

dx.doi.org/10.1021/la5030668 | Langmuir 2014, 30, 11723−11733

peak from the SEC chromatograms demonstrates rapid exchange on a time scale faster than the 20 min required for the elution of the bicelles (Figure S6).

The measurement of ensemble averages in rapid exchange is common in NMR. For instance, structural models of proteins commonly represent an ensemble average of a distribution of structural conformers in rapid exchange.[52] Because we are measuring ensemble-averaged bicelle sizes from a Poisson distribution, we are extracting only effective structural parameters from structural models. The approach used in the following theoretical models will deal with an ensemble average in the distribution of lipid molecules to bicelles.

Bicelle Structural Model. Dynamic light scattering, SANS, SAXS, and cryo-electron microscopy studies have confirmed the discoidal shape of isotropic tumbling bicelles.[53] A simple model can be used to describe the central, cylindrical region and the hemitoroidal rim. Bicelle morphologies are typically described in relation to the surface areas of the central and rim portions,[3,4] but in the approach presented here, we will use bicelle volumes to compare changes in bicelle size in the presence of curvature-inducing molecules.

The volume of the reference bicelle is presented in Table 2. The reference bicelle is composed of a rim and a central region,

Table 2. Curved Bicelle Models and Equations

model	equation
no curvature	
(a) reference bicelle	$V = \pi R^2 h + \pi r^2(2r + \pi R)$
negative curvature	
(b) negative asymmetric central	$V = \frac{1}{18}\pi h(1 - \cos\theta_0)(7h^2 - 24R_c h + 36R_c^2) + \pi r^2\left(2r\cos\theta_0 - \pi\sin\theta_0\left(R_c - \frac{1}{3}h\right)\right)$
(c) negative symmetric central	$V = \pi R^2 h_{eff} + \pi r^2(2r + \pi R)$
positive curvature	
(d) positive rim	$V = \pi R^2 h + \pi r_{eff}^2(2r_{eff} + \pi R)$
(e) positive asymmetric central	$V = \frac{1}{18}\pi h(1 - \cos\theta_0)(7h^2 - 24R_c h + 36R_c^2) + \pi r^2\left(2r\cos\theta_0 + \pi\sin\theta_0\left(R_c - \frac{1}{3}h\right)\right)$
(f) positive symmetric central	$V = \frac{2}{3}\pi(r + R)^2 h$

and the volume depends on the height of the central region, h, the radius of the central region, R, and the radius of the hemitoroidal rim, r. The height of the DMPC bilayer in the central region is 37 Å.[41]

The volumes of the central and rim portions can alternately be calculated from the number of lipids in these regions as well as their molecular volumes. The number of DMPC and bound DHPC molecules in each bicelle is calculated from the q_e ratio and the average size of the bicelle.

$$M_{bicelle} = N_{DHPC}M_{DHPC} + N_{DMPC}M_{DMPC} \quad (12)$$

$$q_e = \frac{N_{DMPC}}{N_{DHPC}} \quad (13)$$

Accurate volumes for DMPC and DHPC molecules determined by crystallographic methods are 1100 and 677 Å^3, respectively.[41]

The reference bicelle volume in Table 2 invokes a high degree of phase separation for the long-chain lipids in the central region and the short-chain, detergent lipids in the rim region.[53] Intermediate cases have been proposed with an oblate globular micellar structure in which there is partial mixing of lipids between these two regions.[54] Lin et al. performed SANS measurements on isotropic bicelles composed of diheptanoylphosphatidylcholine (D7PC) and DPPC and found that a fully phase-separated discoidal bicelle model overestimated the volume of the rim by ca. 68%; therefore, they used an oblate globular micelle model with partial lipid mixing to fit their data.[55] However, their approach used an elliptic hemitoroid to model the rim of their phase-separated discoidal bicelle, which extends the full height of the central, cylindrical region. By contrast, the fully phase-separated volume calculated for the discoidal reference bicelle in Table 2 is consistent with the dimensions in the SANS study.

Translational diffusion experiments on isotropic bicelles further support the phase-separated discoidal model in Table 2. Chou et al. conducted pulse-field-gradient (PFG) NMR experiments on bicelles with DMPC and POPC long-chain lipids and DHPC short-chain lipids with q ratios between 0.15 and 0.53,[15] and they found that these have molecular weights of between 21.7 and 67.2 kDa. The calculated radius of the rim gives a hemitoroidal radius of 13.3 Å for the q = 0.15 bicelles and 13.7 Å for the q = 0.53 bicelles. These are in close agreement with the prolate short axis of 12.5−14.0 Å for a DHPC micelle[42] and make intuitive sense because the long axis extends the circumference of the cylinder at the center of the bicelle. Furthermore, the small variation in this radius suggests that mixing does not increase appreciably as the local concentration of DHPC increases at low bicelle q ratios.

Furthermore, recent studies by Ye et al.[14] and Wu et al.[3] have demonstrated with careful dynamic light scattering and cryo-transmission electron microscopy (cryo-TEM) measurements that isotropically tumbling DHPC/DMPC bicelles with low q ratios ($q \leq 0.5$) form homogeneous, monodisperse disklike particles at lipid concentrations comparable to those used in this study. We have therefore used a discoidal bicelle representation to model the reference bicelle structure.

Perturbing lipids change the structure of bicelles either by partitioning in the rim or the central portion of the bicelle (Figure 4). Bicelles with positive-curvature lipids are consistently smaller than the reference DMPC-bicelles such that their measured B ratios are smaller than 1.0, and foreign lipids with negative curvature are consistently larger such that their measured B ratios are larger than 1.0.

The density of the hydrated phospholipids that compose the reference and curved bicelles is expected to remain constant, and the theoretical B ratios are calculated from the theoretical volumes of the reference and curved bicelles.

$$B = \frac{V_{curved}}{V_{reference}} \quad (14)$$

The B ratios are calculated by comparing the ratio in volumes between the reference bicelle (model a in Figure 4) to those of curved bicelles with negative curvature (models b and c) or positive curvature (models d−f) using the expressions in Table 2.

Positive Curvature. Positive curvature in the rim region is modeled by a change in the effective radius (r_{eff}) of the hemitoroidal rim (model d in Figure 4). Positive-curvature

dx.doi.org/10.1021/la5030668 | Langmuir 2014, 30, 11723−11733

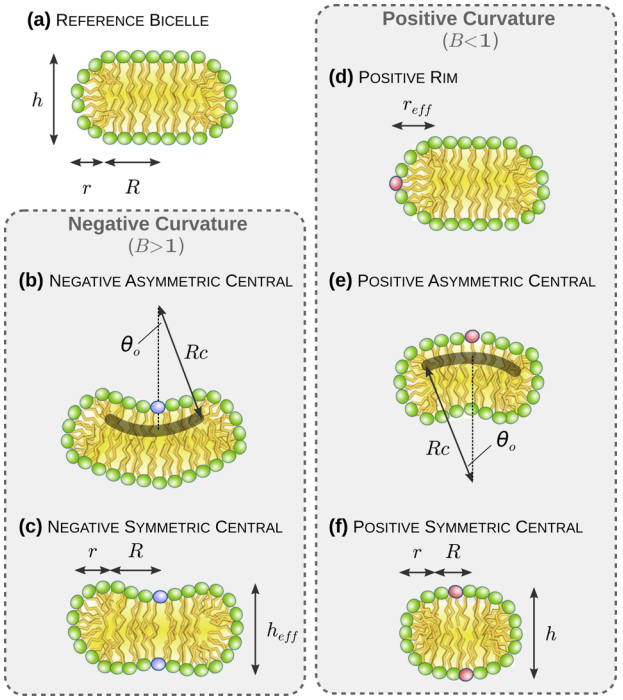

Figure 4. Graphic representation of the reference discoidal bicelle and the curved bicelles induced by a positive-curvature perturbing lipid (b and d, red headgroup) and a negative-curvature perturbing lipid (c, blue headgroup). Phosphocholine headgroups of the membrane are colored in green, and the aliphatic chains are colored in yellow. The central cylindrical region is composed of DMPC, and the rim is composed of DHPC. The illustration is a cut-away lateral profile of the bicelle. The structure and size of the bicelle depend on the radius of the planar central region (R), the height of the central region, and the radius of the hemitoroidal rim (r). See Table 2 for the corresponding volume equations of curved bicelle models.

lipids with a larger radius of curvature will increase r_{eff} when compared to bicelles with an equivalent amount of added DHPC (DHPC-bicelles). At temperatures below 25 °C, the DPC-bicelles illustrate the impact of positive-curvature perturbation on the rim because these bicelles are larger than the DHPC-bicelles. In this regime, the increased size of the DPC-bicelles compared to that of the DHPC-bicelles is consistent with a larger radius of curvature for DPC. DPC forms prolate micelles such as DHPC, and the radius of the short axis is 18.6−19.5 Å for DPC compared to the much shorter 12.5−14 Å for DHPC.[42]

The fit parameters to the bicelle curvature models are presented in Table 3. For the DPC-bicelles at 15 °C, the r_{eff} is ca. 2% larger than the corresponding radius in the DHPC-bicelles. The larger radius of DPC is additionally evident in the larger bicelle size for the DMPC/DPC bicelles in comparison to that for DMPC/DHPC bicelles in our SEC data as well as reports from others.[7]

At temperatures above the phase-transition temperature of DMPC, there is a temperature-dependent reduction in the size of the DPC-bicelles. This reduction in size is consistent with a partial mixing of DPC in the central region of the bicelle. $[DHPC]_{free}$ remains constant at higher temperatures for the DPC-bicelles, in contrast to the increase in $[DHPC]_{free}$ observed for the reference bicelles, indicating that a migration of DPC to the central region increases the affinity of the rim for DHPC molecules. Alternatively, the reduction in size could be due to a concerted decrease in $[DPC]_{free}$ with an increase in $[DPC]_{rim}$ as the sample temperature is increased. However, we consider this possibility unlikely because $[detergent]_{free}$ tends to increase with temperature and a change from the expected 1−1.5 mM $[DPC]_{free}$ would only modestly reduce the q_e ratio and the bicelle size. Furthermore, the increased ^{31}P R_2 rates for DMPC demonstrates a mixing and ordering effect by DPC molecules in the DMPC phase (Figure 2).

Molecules of DPC that partition in the central region could partition either asymmetrically and unevenly between both leaflets or symmetrically and evenly between both leaflets (models e and f, respectively, in Figure 4). In the symmetric model, both leaflets have structures and volumes that change together. Positive curvature produces an outward bulge in the central region, producing a mixed oblate spheroid structure. In the asymmetric model, the volume of one leaflet changes with respect to the other, producing a "puckered" disc shape. This puckered disc has a concave surface with negative curvature and a larger volume and a convex surface with positive curvature and a smaller volume. The volumes of these are defined by a radius of curvature, R_c, and a curvature half-angle, θ_0. The derivation of the volume equations for these models is presented in the Supporting Information.

The B_t ratio of DPC- to DHPC-bicelles is 0.91 ± 0.04 at 35 °C and 0.64 ± 0.03 at 40 °C, and these are 9 and 57% smaller, respectively, than the DHPC-bicelles. In this regime, the average number of DMPC molecules per bicelle is 7.3 at 35 °C and 4.9 at 40 °C. These bicelles are much smaller than the reference bicelle, and the central region is defined by only a few molecules of DMPC. The best representation for these is a mixed micelle with an elliptical spheroid structure (model f in Figure 4). Structural parameters from the fit are presented in Table 3. Although the structure of the DPC-bicelles could, in principle, be described by an asymmetric structure, this model is likely to be present only for larger bicelles with high q ratios

Table 3. Calculated Curvature Parameters from Translational Diffusion Measurements of Bicelles

sample	temperature (°C)	M_w reference bicelle (kDa)	B_t	model parameters[a]
1.8:1 DOPE in q_e = 0.35 bicelles	20.0	20.3	1.07 ± 0.02	*b*: θ_0 = 3.1 ± 0.8°; R_c = −225 ± 60 Å
	30.0	20.3	1.11 ± 0.03	*b*: θ_0 = 4.3 ± 1.1°; R_c = −145 ± 36 Å
0.8:1 DOPE in q_e = 0.54 bicelles	30.0	22.6	1.19 ± 0.02	*b*: θ_0 = 7.9 ± 0.8°; R_c = −86 ± 8 Å
1.9:1 DOPE in q_e = 0.54 bicelles	30.0	22.6	1.38 ± 0.06	*b*: θ_0 = 14.6 ± 2.1°; R_c = −48 ± 7 Å
6.0:1 DOPE in q_e = 0.52 bicelles	30.0	22.6	2.21 ± 0.04	*b*: θ_0 = 39.5 ± 1.1°; R_c = −17 ± 1 Å
1.1:1 OA in q_e = 0.32 bicelles	30.0	16.4	1.11± 0.10	*b*: θ_0 = 5.4 ± 3.4°; R_c = −151 ± 96 Å
1.8:1 DPC in q_e = 0.27 bicelles	35.0	17.2	0.91 ± 0.04	*f*: R = 6.9± 0.4 Å
	40.0	17.2	0.64 ± 0.03	*f*: R = 4.0± 0.3 Å

[a]Curvature models are outlined in Figure 4 and Table 2.

dx.doi.org/10.1021/la5030668 | *Langmuir* 2014, 30, 11723−11733

and well-defined central regions with a large number of DMPC molecules per bicelle.

Negative Curvature. Negative-curvature lipids are expected to partition predominantly in the low-curvature central region of the bicelle rather than the positive-curvature rim. Negative-curvature deformations in the central region can be modeled either by a symmetric or an asymmetric curvature in the two leaflets.

In the negative symmetric central model (model c, Figure 4), both leaflets have structures and volumes that change together. Symmetric negative curvature produces a biconcave central region with an inward cavity in both leaflets. Consequently, the membrane height at the core is smaller than on the outer edges of the central region, and the central region is defined by an effective membrane height, h_{eff}. Because the membrane heights of DOPE and DMPC in the L_α phase are nearly the same,[41,56] this model requires an extensive permeation and enrichment of DHPC in the central region. This is not observed because the DOPE-bicelles do not exhibit a decrease in $[DHPC]_{free}$ in comparison to the reference bicelles, like the DPC-bicelles (Figure S4), nor is this observed for the DOPE titration where increasing amounts of DOPE maintain a constant $[DHPC]_{free}$. Furthermore, the concentration of DHPC molecules in the core of the central region needed to reduce the membrane height would be expected to follow a positive-curvature model like the one presented in model f.

A negative asymmetric central model of curvature (model b, Figure 4) favorably groups the negative-curvature DOPE molecules on the same negative-curvature central leaflet of the bicelle. This type of lipid sorting has been described before in vesicles.[22,24,57] We have therefore modeled the negative curvature of DOPE using asymmetric negative central curvature model b. The calculated radius of curvature, R_c, and half-angle of curvature, θ_0, from translational diffusion are summarized in Table 3. The $q_e = 0.35$ bicelles with an average of 1.8 molecules of DOPE per bicelle have an R_c of -225 ± 60 Å and a θ_0 of $3.1 \pm 0.8°$ at 20.0 °C. At this temperature, the bicelles are 4 °C below the phase-transition temperature of 23.6 °C for DMPC in the L_α state. At 30 °C, 6 °C above the phase-transition temperature of DMPC, these bicelles have an R_c of -145 ± 36 Å and a θ_0 of $4.3 \pm 1.2°$. The greater degree of curvature in the L_α phase is consistent with the more pliable DMPC membrane phase at the higher temperature. The bending modulus of DMPC is about 7 times smaller in the liquid-crystalline phase at 30 °C than in the gel phase at 20 °C.[58]

Because the molecular R_c is known for pure DOPE lipids in water, the effective curvature can be calculated using a hydrophobic insertion model.[59] With molecular areas of 72 $Å^2$ for DMPC and 42 $Å^2$ for DOPE and a molecular R_c of −30 Å for DOPE,[16,24] the calculated effective radius of curvature is between −290 and −580 Å, depending on whether a coupled or uncoupled membrane model is used. The smaller radius of curvature measured in this study indicates a greater degree of curvature for DOPE in the DMPC central region.

The titration of DOPE into the larger bicelles, $q_e = 0.52$, at 30 °C is summarized in Table 3. There is a linear relationship between the average number of DOPE molecules per bicelle and the B_t ratios. At an average of 0.8 molecule of DOPE per bicelle, the R_c is -86 ± 8 Å and the θ_0 is $7.9 \pm 0.8°$, whereas with bicelles that include an average of 6.0 molecules of DOPE, the R_c is -17 ± 1 Å and the θ_0 is $39.5 \pm 1.1°$. The larger $q_e = 0.54$ bicelles exhibit greater curvature with a fewer average number of DOPE molecules than the smaller $q_e = 0.35$ bicelles. For example, $B_t = 1.11 \pm 0.03$ for the $q_e = 0.35$ bicelles with 1.8 molecules of DOPE and $B_t = 1.19 \pm 0.02$ for the $q_e = 0.54$ bicelles with 0.8 molecule of DOPE. This observation shows that the degree of curvature per molecule of DOPE is greater with a larger DMPC surface in the central region of the bicelle.

The OA-bicelles illustrate the pH dependence of negative curvature. The OA-bicelles are matched in lipid composition at pH 7.5 and 4.5, but at the lower pH, the bicelles are $15 \pm 5\%$ ($B_t = 1.15 \pm 0.05$) and $11 \pm 10\%$ ($B_t = 1.10 \pm 0.10$) larger in size at 25 and 30 °C, respectively. At low pH, the oleic acid is protonated and neutral in charge, and thus would be expected to partition more deeply into the bicelle. The increase in bicelle size at low pH indicates the induction of negative curvature that is pH-dependent.

However, the OA-bicelles have a molecular weight that is ca. 19% smaller at pH 7.5 than bicelles with the same q ratio. This observation suggests that the deprotonated form, oleate, induces positive curvature. This observation has previously been confirmed by ESR experiments, which demonstrated that sodium oleate forms micelles at high pH and vesicles at low pH with mixtures of sodium oleate and oleic acid.[60]

CONCLUSIONS

The incorporation of an average of only a few curvature-inducing lipid molecules is sufficient to introduce significant and measurable changes in bicelle size. Complementary diffusion, relaxation, and chromatography measurements demonstrate that these bicelles are homogeneous and monodisperse. DPC reduces the size of bicelles and diffuses to the central region at elevated temperatures. Mixing of DPC and DMPC introduces a considerable ordering in the DMPC lipid dynamics. By constrast, DOPE in bicelles produces bicelles that are considerably larger than reference bicelles. The approach used here, BICS, gives information on the partitioning of lipids and the changes in bicelle size by curvature-inducing molecules, and it is expected to provide future insights into the molecular-level induction of curvature in membranes from proteins and small molecules. Understanding curvature on the molecular level will uncover rich new details to meet the recent and accelerated interest in the biophysics of lipid signaling and trafficking pathways, the rearrangement of lipids, and the fusion and fission of membranes.

ASSOCIATED CONTENT

Supporting Information

Details on the calculation of the free DHPC concentration in bicelles, derivation of the curved bicelle volumes, calibrations of DOSY experiments, 1D spectra of bicelles, sample DOSY decay curves, and a listing of the DMPC ^{31}P relaxation rates for the bicelles. This material is available free of charge via the Internet at http://pubs.acs.org.

AUTHOR INFORMATION

Corresponding Author

*E-mail: justin@lorieau.com.

Author Contributions

The manuscript was written through the contributions of all authors. All authors have given approval to the final version of the manuscript.

Notes

The authors declare no competing financial interest.

■ ACKNOWLEDGMENTS

We acknowledge funding support from the University of Illinois at Chicago and the department of chemistry for this work.

■ ABBREVIATIONS

AFM, atomic force microscopy; BICS, bicelle-induced curvature and sorting; CSA, chemical shift anisotropy; D7PC, diheptanoylphosphatidylcholine; DHPC, dihexanoylphosphocholine; DMPC, dimyristoylphosphocholine; DOPE, dioleoylphosphoethanolamine; DOSY, diffusion-ordered spectroscopy, DPPC, dipalmitoylphosphocholine; DPC, dodecylphosphocholine; ESR, electron spin resonance; LED-BPP, longitudinal eddy current delay, bipolar pulse pair−longitudinal encode/decode; NMR, nuclear magnetic resonance; PFG, pulsed-field gradient; POPC, palmitoyloleoylphosphocholine; RDC, residual dipolar couplings; SANS, small-angle neutron scattering; SAXS, small-angle X-ray scattering; SEC, size exclusion chromatography

■ REFERENCES

(1) Forrest, B. J.; Reeves, L. W. New Lyotropic Liquid Crystals Composed of Finite Nonspherical Micelles. *Chem. Rev.* **1981**, *81*, 1−14.
(2) Liu, Y.; Li, M.; Yang, Y.; Xia, Y.; Nieh, M.-P. The Effects of Temperature, Salinity, Concentration and PEGylated Lipid on the Spontaneous Nanostructures of Bicellar Mixtures. *Biochim. Biophys. Acta* **2014**, *1838*, 1871−1880.
(3) Wu, H.; Su, K.; Guan, X.; Sublette, M. E.; Stark, R. E. Assessing the Size, Stability, and Utility of Isotropically Tumbling Bicelle Systems for Structural Biology. *Biochim. Biophys. Acta, Biomembr.* **2010**, *1798*, 482−488.
(4) Vold, R.; Prosser, R. S. Magnetically Oriented Phospholipid Bilayered Micelles for Structural Studies of Polypeptides. Does the Ideal Bicelle Exist? *J. Magn. Reson. Ser. B* **1996**, *113*, 267−271.
(5) Sanders, C. R.; Prosser, R. S. Bicelles: A Model Membrane System for All Seasons? *Structure* **1998**, *6*, 1227−1234.
(6) Andersson, A.; Mäler, L. Size and Shape of Fast-Tumbling Bicelles as Determined by Translational Diffusion. *Langmuir* **2006**, *22*, 2447−2449.
(7) Lu, Z.; Van Horn, W. D.; Chen, J.; Mathew, S.; Zent, R.; Sanders, C. R. Bicelles at Low Concentrations. *Mol. Pharmaceutics* **2012**, *9*, 752−761.
(8) Li, M.; Morales, H. H.; Katsaras, J.; Kučerka, N.; Yang, Y.; Macdonald, P. M.; Nieh, M.-P. Morphological Characterization of DMPC/CHAPSO Bicellar Mixtures: A Combined SANS and NMR Study. *Langmuir* **2013**, *29*, 15943−15957.
(9) Yamamoto, K.; Pearcy, P.; Ramamoorthy, A. Bicelles Exhibiting Magnetic Alignment for a Broader Range of Temperatures: A Solid-State NMR Study. *Langmuir* **2014**, *30*, 1622−1629.
(10) Bax, A. Weak Alignment Offers New NMR Opportunities to Study Protein Structure and Dynamics. *Protein Sci.* **2003**, *12*, 1−16.
(11) Marcotte, I.; Auger, M. Bicelles as Model Membranes for Solid- and Solution-State NMR Studies of Membrane Peptides and Proteins. *Concepts Magn. Reson., Part A* **2005**, *24A*, 17−37.
(12) Dürr, U. H. N.; Gildenberg, M.; Ramamoorthy, A. The Magic of Bicelles Lights up Membrane Protein Structure. *Chem. Rev.* **2012**, *112*, 6054−6074.
(13) Ujwal, R.; Bowie, J. U. Crystallizing Membrane Proteins Using Lipidic Bicelles. *Methods* **2011**, *55*, 337−341.
(14) Ye, W.; Lind, J.; Eriksson, J.; Mäler, L. Characterization of the Morphology of Fast-Tumbling Bicelles with Varying Composition. *Langmuir* **2014**, *30*, 5488−5496.
(15) Chou, J. J.; Baber, J. L.; Bax, A. Characterization of Phospholipid Mixed Micelles by Translational Diffusion. *J. Biomol. NMR* **2004**, *29*, 299−308.
(16) Zimmerberg, J.; Kozlov, M. M. How Proteins Produce Cellular Membrane Curvature. *Nat. Rev. Mol. Cell Biol.* **2006**, *7*, 9−19.
(17) Kumar, V. V. Complementary Molecular Shapes and Additivity of the Packing Parameter of Lipids. *Proc. Natl. Acad. Sci. U.S.A.* **1991**, *88*, 444−448.
(18) Pomorski, T. G.; Nylander, T.; Cárdenas, M. Model Cell Membranes: Discerning Lipid and Protein Contributions in Shaping the Cell. *Adv. Colloid Interface Sci.* **2014**, *205*, 207−220.
(19) Hallock, K. J.; Lee, D.-K.; Ramamoorthy, A. MSI-78, an Analogue of the Magainin Antimicrobial Peptides, Disrupts Lipid Bilayer Structure via Positive Curvature Strain. *Biophys. J.* **2003**, *84*, 3052−3060.
(20) Smith, P. E. S.; Brender, J. R.; Ramamoorthy, A. Induction of Negative Curvature as a Mechanism of Cell Toxicity by Amyloidogenic Peptides: The Case of Islet Amyloid Polypeptide. *J. Am. Chem. Soc.* **2009**, *131*, 4470−4478.
(21) Hallock, K. J.; Lee, D.-K.; Omnaas, J.; Mosberg, H. I.; Ramamoorthy, A. Membrane Composition Determines Pardaxin's Mechanism of Lipid Bilayer Disruption. *Biophys. J.* **2002**, *83*, 1004−1013.
(22) Callan-Jones, A.; Bassereau, P. Curvature-Driven Membrane Lipid and Protein Distribution. *Curr. Opin. Solid State Mater. Sci.* **2013**, *17*, 143−150.
(23) Wu, Q.-Y.; Liang, Q. Interplay between Curvature and Lateral Organization of Lipids and Peptides/proteins in Model Membranes. *Langmuir* **2014**, *30*, 1116−1122.
(24) Kumar, V. V.; Malewicz, B.; Baumann, W. J. Lysophosphatidylcholine Stabilizes Small Unilamellar Phosphatidylcholine Vesicles. Phosphorus-31 NMR Evidence for the "Wedge" Effect. *Biophys. J.* **1989**, *55*, 789−792.
(25) Leikin, S.; Kozlov, M. M.; Fuller, N. L.; Rand, R. P. Measured Effects of Diacylglycerol on Structural and Elastic Properties of Phospholipid Membranes. *Biophys. J.* **1996**, *71*, 2623−2632.
(26) Fuller, N.; Benatti, C. R.; Rand, R. P. Curvature and Bending Constants for Phosphatidylserine-Containing Membranes. *Biophys. J.* **2003**, *85*, 1667−1674.
(27) Kozlov, M. M. Determination of Lipid Spontaneous Curvature from X-Ray Examinations of Inverted Hexagonal Phases. *Methods Mol. Biol.* **2007**, *400*, 355−366.
(28) Roux, A.; Cuvelier, D.; Nassoy, P.; Prost, J.; Bassereau, P.; Goud, B. Role of Curvature and Phase Transition in Lipid Sorting and Fission of Membrane Tubules. *EMBO J.* **2005**, *24*, 1537−1545.
(29) Parthasarathy, R.; Groves, J. T. Curvature and Spatial Organization in Biological Membranes. *Soft Matter* **2007**, *3*, 24−33.
(30) Sorre, B.; Callan-Jones, A.; Manneville, J.-B.; Nassoy, P.; Joanny, J.-F.; Prost, J.; Goud, B.; Bassereau, P. Curvature-Driven Lipid Sorting Needs Proximity to a Demixing Point and Is Aided by Proteins. *Proc. Natl. Acad. Sci. U.S.A.* **2009**, *106*, 5622−5626.
(31) Stachowiak, J. C.; Schmid, E. M.; Ryan, C. J.; Ann, H. S.; Sasaki, D. Y.; Sherman, M. B.; Geissler, P. L.; Fletcher, D. A.; Hayden, C. C. Membrane Bending by Protein-Protein Crowding. *Nat. Cell Biol.* **2012**, *14*, 944−949.
(32) Brumm, T.; Jørgensen, K.; Mouritsen, O. G.; Bayerl, T. M. The Effect of Increasing Membrane Curvature on the Phase Transition and Mixing Behavior of a Dimyristoyl-Sn-Glycero-3-Phosphatidylcholine/Distearoyl-Sn-Glycero-3-Phosphatidylcholine Lipid Mixture as Studied by Fourier Transform Infrared Spectroscopy. *Biophys. J.* **1996**, *70*, 1373−1379.
(33) Fidorra, M.; Heimburg, T.; Seeger, H. M. Melting of Individual Lipid Components in Binary Lipid Mixtures Studied by FTIR Spectroscopy, DSC and Monte Carlo Simulations. *Biochim. Biophys. Acta, Biomembr.* **2009**, *1788*, 600−607.
(34) Marasinghe, P. A.; Buffy, J. J.; Schmidt-Rohr, K.; Hong, M. Membrane Curvature Change Induced by an Antimicrobial Peptide Detected by 31P Exchange NMR. *J. Phys. Chem. B* **2005**, *109*, 22036−22044.
(35) Wang, T.; Cady, S. D.; Hong, M. NMR Determination of Protein Partitioning into Membrane Domains with Different

Curvatures and Application to the Influenza M2 Peptide. *Biophys. J.* **2012**, *102*, 787−794.
(36) Nichols, J. W.; Ozarowski, J. Sizing of Lecithin-Bile Salt Mixed Micelles by Size-Exclusion High-Performance Liquid Chromatography. *Biochemistry* **1990**, *29*, 4600−4606.
(37) Wider, G.; Dotsch, V.; Wuthrich, K. Self-Compensating Pulsed Magnetic-Field Gradients for Short Recovery Times. *J. Magn. Reson. Ser. A* **1994**, *108*, 255−258.
(38) Delaglio, F.; Grzesiek, S.; Vuister, G. W.; Zhu, G.; Pfeifer, J.; Bax, A. NMRPipe: A Multidimensional Spectral Processing System Based on UNIX Pipes. *J. Biomol. NMR* **1995**, *6*, 277−293.
(39) Skelton, N. J.; Cavanagh, J.; Fairbrother, W. J.; Palmer, A. G., III. *Protein NMR Spectroscopy: Principles and Practice*; Academic Press: San Diego, 1995; p 885.
(40) Koynova, R.; Caffrey, M. Phases and Phase Transitions of the Phosphatidylcholines. *Biochim. Biophys. Acta* **1998**, *1376*, 91−145.
(41) Nagle, J. F.; Tristram-Nagle, S. Structure of Lipid Bilayers. *Biochim. Biophys. Acta* **2000**, *1469*, 159−195.
(42) Lipfert, J.; Columbus, L.; Chu, V. B.; Lesley, S. A.; Doniach, S. Size and Shape of Detergent Micelles Determined by Small-Angle X-Ray Scattering. *J. Phys. Chem. B* **2007**, *111*, 12427−12438.
(43) Wenk, M. R.; Seelig, J. Proton Induced Vesicle Fusion and the Isothermal Lalpha->HII Phase Transition of Lipid Bilayers: A 31P-NMR and Titration Calorimetry Study. *Biochim. Biophys. Acta* **1998**, *1372*, 227−236.
(44) Kay, L. E.; Torchia, D. A.; Bax, A. Backbone Dynamics of Proteins as Studied by 15N Inverse Detected Heteronuclear NMR Spectroscopy: Application to Staphylococcal Nuclease. *Biochemistry* **1989**, *28*, 8972−8979.
(45) Hori, Y.; Demura, M.; Niidome, T.; Aoyagi, H.; Asakura, T. Orientational Behavior of Phospholipid Membranes with Mastoparan Studied by 31P Solid State NMR. *FEBS Lett.* **1999**, *455*, 228−232.
(46) Seelig, J. 31P Nuclear Magnetic Resonance and the Head Group Structure of Phospholipids in Membranes. *Biochim. Biophys. Acta* **1978**, *515*, 105−140.
(47) Roberts, M. F.; Redfield, A. G. High-Resolution 31P Field Cycling NMR as a Probe of Phospholipid Dynamics. *J. Am. Chem. Soc.* **2004**, *126*, 13765−13777.
(48) Habazettl, J.; Wagner, G. A New Simplified Method for Analyzing 15N Nuclear Magnetic Relaxation Data of Proteins. *J. Magn. Reson. Ser. B* **1995**, *109*, 100−104.
(49) Lorieau, J. L.; Louis, J. M.; Bax, A. Whole-Body Rocking Motion of a Fusion Peptide in Lipid Bilayers from Size-Dispersed 15N NMR Relaxation. *J. Am. Chem. Soc.* **2011**, *133*, 14184−14187.
(50) Lipari, G.; Szabo, A. Model-Free Approach to the Interpretation of Nuclear Magnetic Resonance Relaxation in Macromolecules. 1. Theory and Range of Validity. *J. Am. Chem. Soc.* **1982**, *104*, 4546−4559.
(51) Yao, S.; Babon, J. J.; Norton, R. S. Protein Effective Rotational Correlation Times from Translational Self-Diffusion Coefficients Measured by PFG-NMR. *Biophys. Chem.* **2008**, *136*, 145−151.
(52) Wagner, G.; Hyberts, S. G.; Havel, T. F. NMR Structure Determination in Solution: A Critique and Comparison with X-Ray Crystallography. *Annu. Rev. Biophys. Biomol. Struct.* **1992**, *21*, 167−198.
(53) Glover, K. J.; Whiles, J. A.; Wu, G.; Yu, N.; Deems, R.; Struppe, J. O.; Stark, R. E.; Komives, E. A.; Vold, R. R. Structural Evaluation of Phospholipid Bicelles for Solution-State Studies of Membrane-Associated Biomolecules. *Biophys. J.* **2001**, *81*, 2163−2171.
(54) Lin, T.-L. Phase Boundaries of Mixed Short-Chain/long-Chain systems—Predictions of Geometrical Models. *J. Colloid Interface Sci.* **1992**, *154*, 444−453.
(55) Lin, T.-L.; Liu, C. Structure of Mixed Short-Chain Lecithin/Long-Chain Lecithin Aggregates Studied by Small-Angle Neutron Scattering. *J. Phys. Chem.* **1991**, *95*, 6020−6027.
(56) Gruner, S. M.; Tate, M. W.; Kirk, G. L.; So, P. T. C.; Turner, D. C.; Keane, D. T.; Tilcock, C. P. S.; Cullis, P. R. X-Ray Diffraction Study of the Polymorphic Behavior of N-Methylated Dioleoylphosphatidylethanolamine. *Biochemistry* **1988**, *27*, 2853−2866.
(57) Kamal, M. M.; Mills, D.; Grzybek, M.; Howard, J. Measurement of the Membrane Curvature Preference of Phospholipids Reveals Only Weak Coupling between Lipid Shape and Leaflet Curvature. *Proc. Natl. Acad. Sci. U.S.A.* **2009**, *106*, 22245−22250.
(58) Yi, Z.; Nagao, M.; Bossev, D. P. Bending Elasticity of Saturated and Monounsaturated Phospholipid Membranes Studied by the Neutron Spin Echo Technique. *J. Phys.: Condens. Matter* **2009**, *21*, 155104.
(59) Campelo, F.; McMahon, H. T.; Kozlov, M. M. The Hydrophobic Insertion Mechanism of Membrane Curvature Generation by Proteins. *Biophys. J.* **2008**, *95*, 2325−2339.
(60) Fukuda, H.; Goto, A.; Yoshioka, H.; Goto, R.; Morigaki, K.; Walde, P. Electron Spin Resonance Study of the pH-Induced Transformation of Micelles to Vesicles in an Aqueous Oleic Acid/Oleate System. *Langmuir* **2001**, *17*, 4223−4231.